Adsorption of Biopolymers on SWCNT: Ordered Poly(rC) and Disordered Poly(rI)

ARTICLE *in* THE JOURNAL OF PHYSICAL CHEMISTRY B · MARCH 2013

Impact Factor: 3.3 · DOI: 10.1021/jp311005y · Source: PubMed

5 AUTHORS, INCLUDING:

Maksym Karachevtsev
B.Verkin Institute for Low Temperature Physic…
19 PUBLICATIONS **195** CITATIONS
SEE PROFILE

Galina Gladchenko
National Academy of Sciences of Ukraine
38 PUBLICATIONS **238** CITATIONS
SEE PROFILE

Victor Karachevtsev
National Academy of Sciences of Ukraine
79 PUBLICATIONS **470** CITATIONS
SEE PROFILE

THE JOURNAL OF PHYSICAL CHEMISTRY B

Article

pubs.acs.org/JPCB

Adsorption of Biopolymers on SWCNT: Ordered Poly(rC) and Disordered Poly(rI)

Maksym V. Karachevtsev,* Galina O. Gladchenko, Alexander M. Plokhotnichenko, Victor S. Leontiev, and Victor A. Karachevtsev

B. I. Verkin Institute for Low Temperature Physics and Engineering, National Academy of Sciences of Ukraine, 47 Lenin Avenue, 61103 Kharkov, Ukraine

ABSTRACT: Polymer adsorption onto single-walled carbon nanotubes (SWCNTs) depends on its rigidity/flexibility. The adsorption properties of two related homopolynucleotides poly(rI) and poly(rC) but of different rigidities were compared, employing absorption spectroscopy and molecular dynamics simulation. It was shown that adsorption of the poor base stacked poly(rI) onto the nanotube is less effective than that of the strong base stacked poly(rC), the chain of which is of higher rigidity. Analysis of UV absorption spectra of polymer:nanotube suspension at heating until 90 °C, which leads to partial nanotube aggregation because of the weakly bound polymer sliding from the tube surface, revealed that the percent of precipitated nanotubes in suspension with poly(rI) is larger than that in suspension with poly(rC) (16% vs 7%). This fact indicates the higher stability of SWCNT:poly(rC) hybrid in comparison with SWCNT:poly(rI). Less effective adsorption of poly(rI) is confirmed with a weaker hypochromic effect of nanotubes covered with poly(rI) than with poly(rC), which originates from $\pi-\pi$ stacking of nitrogen bases with the nanotube surface. Spontaneous adsorption of oligomers on the nanotube simulated by the molecular dynamics showed that oligomer $r(I)_{25}$ has a weaker energy of binding to the carbon nanotube surface than $r(C)_{25}$. The oligomer with ordered bases has a tendency to form the stretched conformation along the nanotube, which provides a higher binding energy, while more flexible $r(I)_{25}$ forms the stable loop spaced away from the nanotube surface, the stability of which is strengthened with H-bonding between bases.

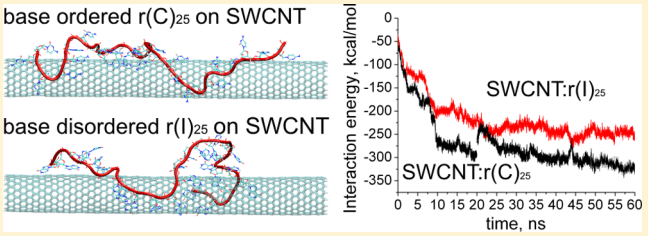

INTRODUCTION

Due to their unique mechanical, electronic, and optical properties, single-walled carbon nanotubes (SWCNTs) are among the most promising nanomaterials for technological applications in electronics, new composite materials, energy conversion devices, different sensors, and biomedical applications. Polymers conjugated with SWCNTs facilitate their application in advanced technology.[1] Noncovalent binding of the polymer to the carbon nanotube surface is remarkable for dispersing SWCNTs in organic solvents[2] and water,[3,4] for producing unusual nanohybrids used in biochemistry and biosensing, and for creating nanocomposites with reinforced mechanical properties of the bulk material due to the extraordinary strength of nanotubes.

A variety of polymer structures dictates different conformations of the polymer adsorbed to SWCNT. Some success in creating a strong nanohybrid formed with the polymer and nanotubes has been achieved when the polymer was wrapping around nanotubes.[1,5] As it was shown with computer simulation, this effect depends on the rigidity/flexibility of polymer species and on their affinity to the SWCNT surface.[6−10]

Employing Monte Carlo simulations, Srebnik et al. found that, in addition to the highly curved surface of SWCNTs, the chain stiffness is sufficient to induce helical wrapping.[7,8] Both van der Waals[6] and $\pi-\pi$ stacking[3] interactions play a significant role in promoting helical wrapping of various polymers around SWCNTs. Then, they indicated that the ordered conformations arise from a balance between conformational energies, entropic penalties, and intramolecular and intermolecular interactions. Also, other researchers concluded that a combination of backbone stiffness and $\pi-\pi$ interactions with SWCNTs can stabilize the polymer adsorption on the nanotube surface.[2,9,10]

Recently, Tallury and Pasquinelli simulated binding of the stiff and flexible polymer to carbon nanotubes.[9,10] The simulations showed that polymers with flexible backbones prefer to wrap around SWCNT, although not in any distinct conformation.[9] They did not observe helical conformations of this polymer, while polymers with stiff and semiflexible backbones tend to wrap around the SWCNT with more distinct conformations.[10] It was also demonstrated that aromatic moieties along the backbone appear to dictate the adsorption conformation which is likely due to the preference for optimizing $\pi-\pi$ interactions.

Among many polymers interfaced with SWCNTs, single-stranded DNA (ss-DNA) is the most popular and intriguing polymer with promising perspectives in biomedicine and biosensing.[3,4,11−29] Due to its helical structure, DNA can

Received: November 7, 2012
Revised: February 6, 2013
Published: February 11, 2013

   dx.doi.org/10.1021/jp311005y | J. Phys. Chem. B 2013, 117, 2636−2644

wrap tightly around the nanotube in water spontaneously. As ss-DNA in aqueous solution carries a negative charge in the chain and also contains hydrophobic components, the stable hybrid with the nanotube is created when hydrophobic nitrogen bases (NBs) are adsorbed to the nanotube surface via $\pi-\pi$ stacking, while the hydrophilic sugar−phosphate backbone is directed to water.[3] ss-DNA involves a set of polymers with slightly different physical properties (rigidity, thermostability, and so on), which can be created by varying the sequence of NBs. Thus, these related polymers give the unique possibility of the fine modulation of the polymer interaction with SWCNT, changing the base type[29] or their sequence.[3] Recent research gave an opportunity to hope that each polymer binds most effectively only to the nanotube of the certain chirality or diameter.[21,22,25] Thus, it should rely on the separation of nanotubes with certain chirality from the bulk material by choosing an appropriate DNA sequence.

Models of hybrids formed with ss-DNA and the nanotube with different structural parameters were simulated by molecular dynamics (MD) modeling.[3,12−24] These simulations indicate that ss-DNA binding to SWCNT is very strong. The calculation confirms that $\pi-\pi$ stacking between NBs and the nanotube surface is the basic mechanism of the interaction between SWCNT and DNA and the major reason for the hybrid stability. Accurate quantum-chemical methods applied for describing these interactions provided a quantitative characterization of the mechanism of DNA binding to the nanotube surface.[26−28] The stability row of SWCNT:NBs was established: guanine (G) > adenine (A) > cytosine (C) ≈ thymine (T) > uracil (U).

The $\pi-\pi$ stacking interaction between the nanotube sidewall and NBs influences the absorption spectrum of bound polymer.[30] It is known that the absorption intensity of π-stacked compounds decreases because of changes in the electronic interactions between them[31] (the so-called hypochromic effect[32]). Theory considers hypochromicity as a result of the weak dipole−dipole interactions between stacked flat organic compounds with the π-system modified by the light wave.[31] The hypochromic effect is distinctly observed in the case of DNA, the UV absorption of which decreases when two single strands form the duplex structure.[31,32] Recently, Hughes et al.[30] have studied UV−visible absorption spectra of 30-base-long homooligonucleotides wrapped around the SWCNT in aqueous suspension. As the polymer absorption spectrum is mainly conditioned with absorption of NBs (see, for example, ref 32) in the UV range from 200 to 300 nm, they observed a significant transformation of absorption spectra of different homooligonucleotides after their adsorption on the nanotube surface. The $\pi-\pi$ stacking interaction between the nanotube and π-conjugated NBs was directly manifested not only in the DNA absorption spectrum but was also observed in the absorption spectrum of polymer-wrapped SWCNTs.[33] It was demonstrated that at wavelengths longer than 300 nm the absorption spectrum of the polymer-wrapped SWCNTs was of weaker absorption intensity than the spectrum of unbound SWCNTs.

Here, we investigate the adsorption of two relatively long homopolynucleotides, polyriboinosinic acid (poly(rI)) and polyribocytidylic acid (poly(rC)) (Figure 1) on the SWCNT surface, employing absorption spectroscopy and MD simulation. These two related polymers possess the same sugar−phosphate backbone but differ only in the structure of the bases. It is known that these polymers have different base

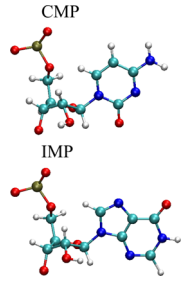

Figure 1. Structures of inosine monophosphate (IMP) and cytidine monophosphate (CMP). The nitrogen, hydrogen, phosphorus, carbon, and oxygen atoms are depicted by blue, white, tan, cyan, and red, respectively.

ordering at room temperature and, therefore, different rigidity. Thus, poly(rC) has high ordering,[34−36] while the structure of poly(rI) is characterized as quite disordered.[37−39] Adsorption of the first biopolymer on the nanotube surface has been simulated earlier.[23] Recently, a quantitative comparison of the relative ability of "wrapping polymers" including oligonucleotides to disperse SWCNTs in water was carried out.[4] This comparison showed that $d(C)_{20}$ or $d(C)_{30}$ is an efficient dispersion agent. Another experimental study demonstrated that nanotubes were highly exfoliated and temporally stable in $d(C)_{15}$ and/or $d(T)_{15}$ surroundings.[29] The time dependent fixed temperature experiments that probe the kinetics of the biopolymer dissociation from the nanotube surface allowed the order of the strength of the nucleobase binding to SWCNTs to be ascertained as G > C > A > T.[40] In addition to these studies, the investigation of the hypochromic effect of polymer-wrapped SWCNTs, observed in the absorption spectrum, showed the effective poly(rC) binding to the nanotube surface.[33] However, adsorption of poly(rI) on SWCNTs has not been investigated yet. Thus, the main purpose of this work was to study the adsorption of poly(rI) to SWCNTs and to compare this adsorption with that of poly(rC) differing in rigidity.

MATERIAL AND METHODS

Materials. Potassium salts of poly(rC) and poly(rI) acids were purchased from Sigma-Aldrich (USA) and used as received. Polymers were dissolved in aqueous buffer solution consisting of 5×10^{-3} M Na^+ cacodylate (pH 6.9) (Serva, Germany) and 5×10^{-3} M NaCl. Deionized water with 18 MΩ resistance was used in all experiments. The concentration of polynucleotides was determined optically, using the corresponding molar extinction coefficients: poly(rC), ε_{268} = 6300 $M^{-1}\cdot cm^{-1}$;[33,34] poly(rI), ε_{248} = 10100 $M^{-1}\cdot cm^{-1}$.[39]

Purified SWCNTs (produced by the HIPCO method) were purchased from Unidym (USA). In order to obtain SWCNT:RNA conjugates, the carbon nanotubes were mixed with an aqueous solution of polyribonucleotides and were sonicated for 40 min (1 W, 44 kHz). The polymer concentration was 0.4−0.6 mM, and the SWCNT:polymer weight concentration ratio ranged from 1:1 to 1:1.2. After sonication, the suspension was centrifuged at 70 000*g* for 1 h. The supernatant was decanted and used as a stock solution in the experiments. As follows from our former electrophoretic estimation, after 40 min of ultrasonication, the lengths of polymer fragments were within 100−150 nucleotides.[15] An aqueous suspension of SWCNTs with an anionic surfactant sodium dodecyl sulfate (SDS) (Sigma-Aldrich, USA) was

dx.doi.org/10.1021/jp311005y | J. Phys. Chem. B 2013, 117, 2636−2644

prepared by the same method. The surfactant concentration in suspension was 1%.

Methods. *Absorption Spectroscopy.* All UV−visible absorbance measurements were carried out on a Specord M40 (Carl Zeiss, Jena, Germany) equipped with a thermoelectrically controlled cuvette holder. Quartz cuvettes with 1 mm path length were used in the experiments. Absorption spectra were recorded in the range 200−900 nm at room temperature. The temperature dependence of changes in the optical density ($\Delta A(T)$) of polynucleotide (the melting curve) was measured with a heating rate of 0.25 °C/min at λ = 268 nm (poly(rC)) and 248 nm (poly(rI)). In these measurements, a two-cuvette arrangement was used: one cell with nanotube suspension (or polymer solution) was placed and heated in the working channel of the spectrophotometer, while the reference cuvette with a buffer solution was thermostatted within 20 ± 0.5 °C.

Molecular Dynamics Simulation. Adsorption of homooligonucleotides $r(I)_{25}$ and $r(C)_{25}$ on the SWCNT surface was simulated by the molecular dynamics method. For this purpose, the program package NAMD[41] was employed with the Charmm27 force field parameter set.[42] Periodic boundary conditions were applied in modeling. Sizes of boxes were 52 Å × 66 Å × 141 Å and 51 Å × 65 Å × 141 Å for SWCNT:$r(I)_{25}$ and SWCNT:$r(C)_{25}$, respectively. Each system was embedded in water (more than 13200 H_2O molecules). The TIP3P water model was used for solvation, and 25 Na^+ ions were added to each system for neutralization of the charge on the sugar−phosphate backbone. The SWCNT for both systems was selected as a zigzag (16,0) nanotube. Its length and diameter were 11.0 and 1.122 nm, respectively. In our simulation, SWCNT atoms were uncharged. The structure of SWCNT was built by a homemade program, and structures of $r(I)_{25}$ and $r(C)_{25}$ were generated by the make-na program.[43] Before the simulation started, the oligonucleotides were located near the nanotube surface (aligned parallel to the SWCNT axes). The SWCNT and oligomer were separated with 2.5 Å distance (defined as the distance between the SWCNT surface and the polymer's nearest atom) for both systems. Oligonucleotides were initialized in the B-conformation. The system was minimized during 1000 steps (with 1 fs time step) and then was modeled during 60 ns (the time step was also 1 fs). In our simulations, the NPT ensemble was used in which the number of molecules, pressure, and temperature were fixed. The temperature and pressure in the periodic boxes were 343 K and 1 atm, respectively. As the temperature rise increases the rate of achieving the energy-favorable conformation of the oligonucleotide on the nanotube, we select the moderate temperature (343 K) which breaks the base self-stacking but is not very high to lead to the oligonucleotide desorption from SWCNT.[23] Interaction energies were calculated by the NAMD Energy Plugin (Version 1.3) which was implemented in the VMD Program package.[44]

RESULTS AND DISCUSSION

Comparison of $r(I)_{25}$ and $r(C)_{25}$ Adsorption on Carbon Nanotubes: Absorption Spectroscopy. Some homopolynucleotides at room temperature, neutral pH, and low ionic strengths have the ordered helical structure which arises because of essential stacking interactions favoring the parallel orientation of adjacent bases.[45] Stacking interactions between NBs are predicted to be the driving force for the formation of ordered helical conformations of homopolynucleotide single strands.[31,45,46] Poly(rC) in water solution with pH ranging from 5.7 to 7 forms a single-stranded right-handed helix with 1.3 nm diameter.[35] The maximally ordered stacking structure is formed only at very low temperatures (near 0 °C).[32] At room temperature, the polymer is in such a conformation when random-coil domains alternate with rigid helical ones.[32,45,46] In the case of poly(rI), the situation is different; this polymer has no stable form of helix,[37−39] which indicates its flexibility. Earlier experiments on CD spectroscopy showed that at neutral pH and low ionic strength poly(rI) is a single-stranded poor base stacked helix.[37]

The ordered structure of the polynucleotide manifests itself in the rise of the optical absorption intensity in the UV range upon the heating of polynucleotide aqueous solution from room temperature to 90 °C as it was observed for poly(rC) (Figure 2). This absorption intensity rise is related to the so-

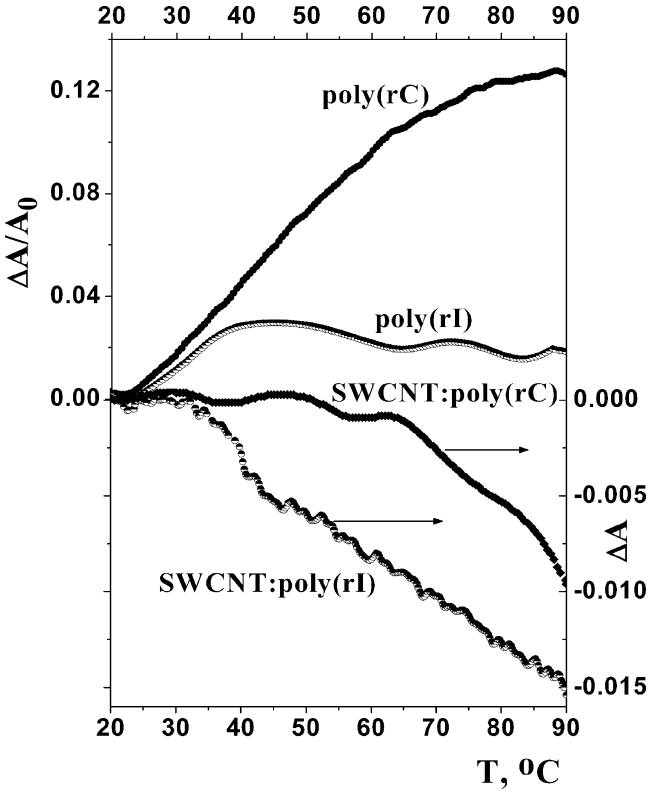

Figure 2. Temperature effect on optical absorption of free poly(rC) and poly(rI) and their hybrids with SWCNTs (measured at 259 and 248 nm, respectively).

called hyperchromic effect. At polymer heating, NBs are disordered, and as a result, decrease of light absorption is taken off. This attenuation (i.e., the hypochromic effect which is opposite the hyperchromic one) appears due to the weak interaction between the dipole moment of the electronic transition of one molecule which absorbed photon and the dipole moment induced in the neighboring molecules.[31,32]

In the double-stranded DNA (ds-DNA), $\pi-\pi$-stacked disordering of bases occurred also when the temperature of the polymer solution increased. This disordering is accompanied with an increase in the optical absorption, which has a characteristic S-like dependence on the temperature (the so-called melting curve) due to high cooperativity of the helix−coil transition in ds-DNA.[31,32] For single-stranded polynucleotides,

dx.doi.org/10.1021/jp311005y | J. Phys. Chem. B 2013, 117, 2636−2644

such S-like temperature dependence is not observed; however, for some polymers, a smooth increase of optical absorbance can be observed, which indicates a more gradual unfolding which assumes a predominantly noncooperative helix−coil transition. For poly(rC), the normalized absorbance change ($\Delta A/A_0$) increases with the temperature growth in the wide temperature range and reaches 13% at 90 °C (Figure 2). It is supposed that at this temperature poly(rC) acquires a practically disordering conformation. However, in poly(rI), $\Delta A/A_0$ increase with temperature is practically absent (Figure 2), which points out the poor base ordering already at room temperature.

Upon the polymer adsorption on the nanotube surface, the base self-stacking ordering is broken down. The absorption intensity of the adsorbed polymer does not rise with the temperature but decreases for both nanotube suspensions (Figure 2). For SWCNT:poly(rI) suspension, this attenuation is observed just with the temperature increase, while for SWCNT:poly(rC) the intensity decrease begins to be noticeable only after $T > 60$ °C. These events are accompanied by the decrease of the nanotube concentration in suspension at heating, which was estimated from the decrease of their inherent absorption (at 730 nm). At 90 °C, this attenuation is 16 and 7% for SWCNT:poly(rI) and SWCNT:poly(rC), respectively. Evidently, the absorption intensity decrease of nanotubes is caused by their precipitation induced with the polymer sliding down from the nanotube surface upon heating and with following the bundle formation. A higher percentage of the bundle formation in SWCNT:poly(rI) suspension indicates that the binding energy of this polymer to the nanotube is lesser than in the case of poly(rC). Note that the increase of the absorption intensity of the polymers is not observed, although it should appear because of the breaking of $\pi-\pi$ stacking interaction between the nanotube and π-conjugated nitrogen bases at heating. This absorption increase (the hyperchromic effect) is compensated with the nanotube absorption decrease owing to their precipitation, which have absorption in this spectral range (240−260 nm) too. We could observe this effect only upon comparison of differential absorption spectra of SWCNT:poly(rI)−SWCNT:SDS, detected at room temperature and 90 °C (Figure 3). Note that the differential spectrum obtained at room temperature characterizes the bound poly(rI). Measured at this temperature, the absorption spectrum of the unbound poly(rI) is shown in Figure 3 too for comparison.

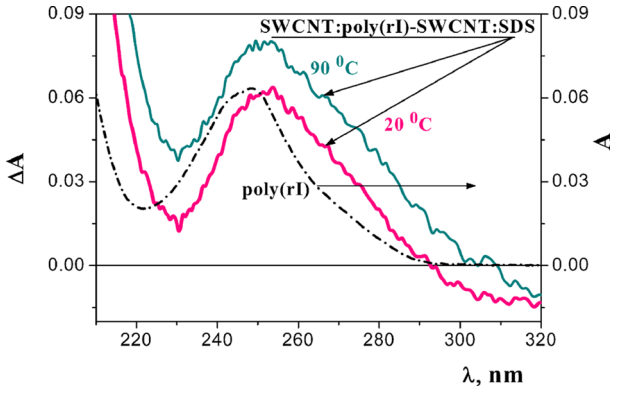

Figure 3. UV absorption spectra of poly(rI) (black) and SWCNT:poly(rI)−SWCNT:SDS, observed at room temperature (red) and 90 °C (green). The poly(rI) spectrum was scaled to the equal peak intensity of the bound poly(rI) spectrum.

The hypoxanthine (nitrogen base of poly(rI)) absorption spectrum is conditioned with two main $\pi \rightarrow \pi^*$ electronic transitions observed at 266−276 and 246−250 nm.[38,39] Upon the comparison of the bound poly(rI) spectrum with that of the free polymer (Figure 3, red and black, respectively), weak differences are seen, namely, the bathochromic shift of the intensive band maximum (248 → 253 nm) and the shoulder appearance in the 266−276 nm region. A similar spectrum transformation was observed earlier for $d(G)_{30}$ adsorbed to the nanotube surface.[30] Note that the base of this oligomer (guanine) and poly(rI) (hypoxanthine) have similar structures (the lack of the amino group in hypoxanthine, as compared to guanine). As the data on the direction and spectral position of optical dipole transitions for hypoxanthine are absent in the literature, we take advantage of the similar structure with guanine and believe that the transition at ∼248 nm corresponds to the long axis of hypoxanthine which aligns along the nanotube axis. In this case, the red-shift of this band after poly(rI) adsorption indicates that hypoxanthines are stacked with the nanotube in such a configuration to align with the direction of the 248 nm transition dipole moment along the nanotube axis as it was observed earlier for $d(G)_{30}$.[30]

The $\pi-\pi$ stacking interaction between the nanotube and π-conjugated NBs, being manifested in transformation of the DNA absorption spectrum, was observed earlier.[30] The appearance of this interaction was also revealed in the absorption spectrum of polymer-wrapped SWCNTs.[33] The polynucleotide interaction with SWCNT induces the decrease of the carbon nanotube absorption intensity in the 300−400 nm region, in comparison with absorption of SWCNTs covered with SDS which has no π-conjugated system. Earlier, we observed this effect for SWCNTs covered with poly(rC), poly(rG), ds-DNA, and ss-DNA.[33] It was shown that the magnitude of the so-called hypochromic coefficient may be used for the comparison of $\pi-\pi$ stacking interactions of different polymers with the nanotube surface.

In this work, we performed a similar analysis of absorption spectra of SWCNT:poly(rI) hybrids in the 200−600 nm region and compared them with those of SWCNT:SDS as well as of the unbound polymer (Figure 4). As SDS absorption in the UV region begins at a wavelength less than 200 nm, the spectrum of SWCNT:SDS aqueous suspension, observed in the 200−600 nm range, is caused only by nanotube absorption. On the contrary, the absorption spectrum of SWCNT:polymer suspension in the range 200−300 nm is a result of superimposition of nanotube and polymer absorption spectra. Absorption spectra of the samples studied are similar in the range 400−600 nm but differ in the intensity. This difference is conditioned with different nanotube concentrations in aqueous suspensions. To compare the nanotube spectra obtained, the spectrum intensity of the polymer-wrapped nanotubes was scaled to their spectrum intensity in SDS environment (Figure 4a), using the multiplier (wavelength independent). In this case, a possible small shift of nanotube spectral peaks, induced by various environments, can be neglected.

As the spectra of the polymer and nanotubes are superimposed in the range 200−300 nm, the corrective extraction of the polymer spectrum from the common one is not a simple procedure because of ambiguity in the determination of polymer and nanotube concentrations. Thus, to take the SWCNT hypochromic effect into account correctly, we do not consider this spectral range.

dx.doi.org/10.1021/jp311005y | J. Phys. Chem. B 2013, 117, 2636−2644

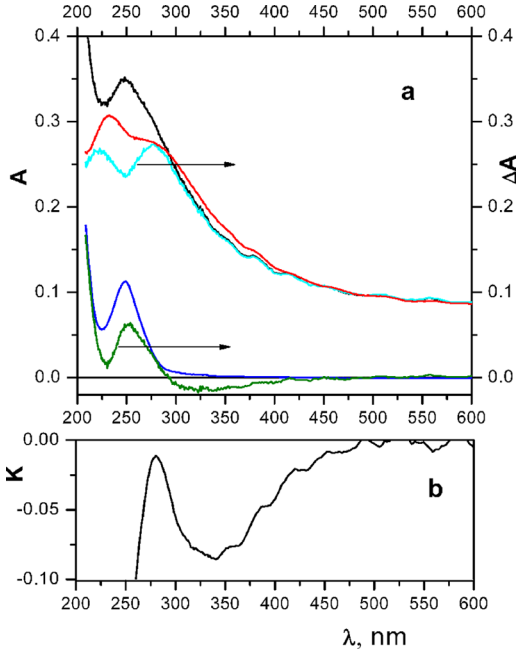

Figure 4. UV−visible absorption spectroscopy determination of SWCNT hypochromism: (a) Absorption spectra of aqueous suspensions of SWCNT:SDS (red) and SWCNT:poly(rI) (black), absorption spectrum of poly(rI) (blue), differential spectra (ΔA) of SWCNT:poly(rI)−poly(rI) (cyan) and SWCNT:poly(rI)−SWCNT:SDS (green). The intensity of the SWCNT:poly(rI) spectrum was normalized to the SWCNT:SDS one in the 500−600 nm spectral range. (b) Spectral dependence of the hypochromic coefficient $-K(\lambda)$ of poly(rI)-covered SWCNT.

As follows from Figure 4, the scaled optical density of SWCNT:poly(rI) suspension in the 300−400 nm range is somewhat lower than that for the SWCNT:SDS ones. It should be noted that the value of the spectra discrepancy decreases monotonically with increasing wavelength. The spectrum of nanotubes interacting with the polymer is obtained by subtracting the poly(rI) spectrum from that of SWCNT:poly-(rI). The differential spectrum is shown in Figure 4a too (remember that the spectrum is correct only at wavelengths more than 300 nm).

The spectrum of the bound poly(rI) (Figure 4a, green) was obtained by subtraction of the "pure" SWCNT spectrum (Figure 4a, red) from that of SWCNT:poly(rI) (Figure 4a, black). To reveal the spectrum transformation of poly(rI) after its adsorption, the spectra of free (Figure 4a, blue) and bound polymers were compared.

The hypochromic effect of SWCNT can be described by the hypochromic coefficient determined as $K(\lambda) = (A_{NTi}(\lambda) - A_{NT}(\lambda))/A_{NT}(\lambda) = (A_{PNT}(\lambda) - A_P(\lambda) - A_{NT}(\lambda))/A_{NT}(\lambda)$ (where $A_{NT}(\lambda)$ and $A_{NTi}(\lambda)$ are spectra of unbound nanotubes (in SDS environment) and nanotubes interacting with the polymer, respectively; $A_{PNT}(\lambda)$ is the spectrum of the nanotubes:polymer sample).[33] As follows from Figure 4, the coefficient $-K(\lambda)$ begins to grow noticeably from 500 nm and reaches a −0.08 value up to 340 nm. Such a monotonous growth of $K(\lambda)$ absolute value upon the wavelength decrease can be explained by the increasing interaction between electronic levels of nanotubes and hypoxanthine as the levels approach each other (see ref 33 for details).

As in the case of poly(rI), poly(rC) interaction with SWCNTs also induces hypochromicity in the 300−500 nm region, in comparison with SWCNT:SDS.[33] We compared spectral dependences of hypochromic coefficients obtained for SWCNT:poly(rI) and SWCNT:poly(rC) suspensions, which were plotted in Figure 5. Note that reliable comparison of the

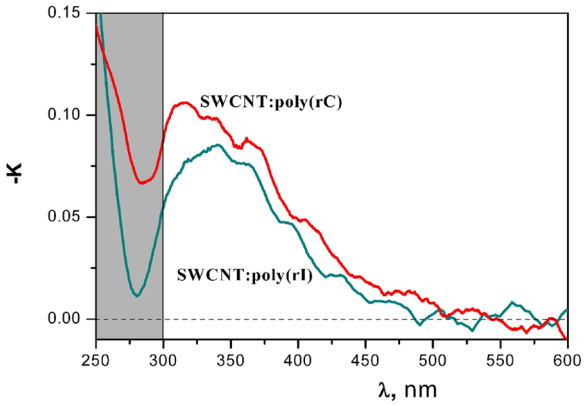

Figure 5. Spectral dependence of the hypochromic coefficient $-K(\lambda)$ of SWCNTs covered with poly(rC) (red) and poly(rI) (green).

$-K(\lambda)$ value can be deduced at wavelengths longer than 300 nm, where absorption spectra of nanotubes and the polymer are not superimposed. It is seen from Figure 5 that the dependence $-K(\lambda)$ for SWCNT:poly(rI) in the range 300−450 nm runs essentially lower than this dependence for SWCNT:poly(rC), and this points to a weaker energy of poly(rI) binding to SWCNTs than was observed for poly(rC).

Comparison of $r(I)_{25}$ and $r(C)_{25}$ Adsorption on Carbon Nanotubes: Molecular Dynamics Simulation. In the initial step of the computer modeling, ribooligonucleotide in the self-ordering helical B-form was located near the carbon nanotube surface in such a configuration that the SWCNT axis was aligned parallel to helix ones, and then the simulation started (Figure 6). During simulation, we monitored every 10 ns the structure of the hybrid obtained, the interaction energy between the SWCNT and oligonucleotide, and the averaged distance between the nearest pair of negatively charged phosphate ions. The initial structure of oligomer $r(I)_{25}$ was selected as the ordered helix because the degree of its disordering is unknown. It should be noted that $r(I)_{25}$

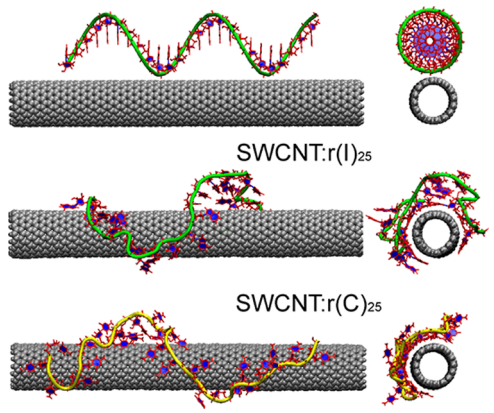

Figure 6. Snapshot of $r(I)_{25}$ structure and SWCNT (16,0) in the initial simulation step, SWCNT:$r(I)_{25}$ and SWCNT:$r(C)_{25}$ hybrids after 60 ns simulation. Water molecules and Na^+ counterions were removed for better visualization. The phosphate backbone is depicted by green and yellow solid curves for $r(I)_{25}$ and $r(C)_{25}$, respectively.

dx.doi.org/10.1021/jp311005y | J. Phys. Chem. B 2013, 117, 2636−2644

disordering and its adsorption on the nanotube surface occurred simultaneously.

As a result of the interaction with the tube surface, the initial oligomer conformation changes essentially even during the first nanoseconds. At that the polymer helix is deformed strongly; this is confirmed with decreasing of the average distance between neighbor phosphates (D_{P-P}) (Figure 7). Thus, for the

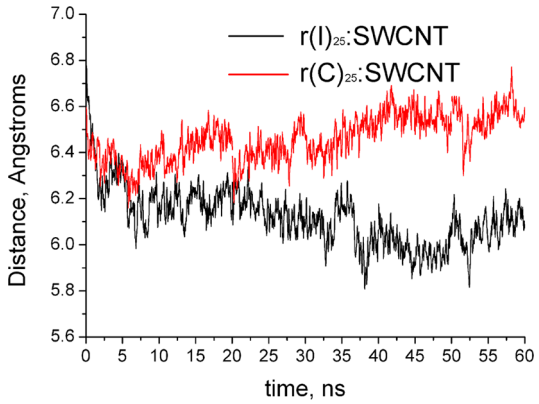

Figure 7. The average distance between neighbor phosphates (D_{P-P}) of $r(C)_{25}$ (red) and $r(I)_{25}$ (black) adsorbed to SWCNT as a function of simulation time.

first nanoseconds, the distance for $(rC)_{25}$ decreases quickly (D_{P-P} varied from 6.6 to 6.4 Å); then, the rate of D_{P-P} change lowers, reaching 6.3 Å in 10 ns. Note that oligomer $r(I)_{25}$ demonstrates more essential transformations of the helix than $(rC)_{25}$, in such a way that D_{P-P} decreases up to 6.1 Å for 10 ns. After 5 ns, D_{P-P} for $r(C)_{25}$ begins to rise and to 40 ns achieves its initial value (~6.6 Å). At the same time, D_{P-P} for $(rI)_{25}$ continues its decreasing and reaches the minimum value (6.0 Å) after 45 ns. After this time, D_{P-P} for this oligomer began to increase, and to the modeling end, the difference in D_{P-P} for two oligomers was 0.4 Å (Figure 7). This evidences that for $r(I)_{25}$ the electrostatic energy of repulsion between phosphate charges is more than that for $r(C)_{25}$ for which the value of this energy is about the same quantity as that for the initial helix. The higher value of repulsive electrostatic energy for $r(I)_{25}$ oligomer adsorbed onto the tube indicates a higher degree of its deformation. Also, higher deformation of this oligomer, in comparison with that of $r(C)_{25}$, can be seen in Figure 6. Thus, the distance between phosphate groups of the beginning and the end of $r(I)_{25}$ after adsorption onto the tube is about 2 times shorter than the same distance for $r(C)_{25}$, which extended by about 20% in comparison with the initial value.

As follows from the above discussion, during the first ns of simulation time, the essential oligomer disordering takes place after adsorption, and as a result, the mean distance between phosphates decreases and the electrostatic repulsion energy within the backbone rises. With time for the $r(C)_{25}$ oligomer, this distance returns to its initial value, but for $r(I)_{25}$, it has a lesser value even after 60 ns of simulation; therefore, the increased electrostatic repulsion hinders this oligomer to achieve the favorable conformation on the nanotube surface.

As the area of pyrimidines (in our case cytosine) containing a single aromatic ring is smaller than the area of purine (in our case hypoxanthines, two rings) and as the $\pi-\pi$ stacking energy rises with increasing surface area of the interacting molecules,[32] the energy of cytosine binding to SWCNT (−50 kJ/mol in a vacuum[27]) is weaker than the energy of hypoxanthine (6-oxopurine) with SWCNT (−68 kJ/mol in a vacuum[27]). However, our simulation shows that, during the first nanoseconds of simulation, binding energies of $r(C)_{25}$ and $r(I)_{25}$ with SWCNT are about equal (Figure 8). Then, with time, this

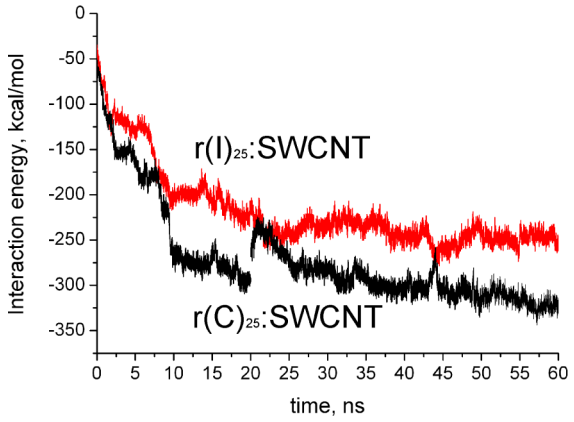

Figure 8. Interaction energies for SWCNT and $r(C)_{25}$ (black) and SWCNT and $r(I)_{25}$ (red) as a function of simulation time.

competition in the interaction energy for benefit of $r(C)_{25}$ takes place, which is explained with the higher number of cytosines stacked with the tube than that of hypoxanthines.

We considered the adsorption process in detail, paying attention to the number of bases stacked to SWCNT in every oligomer and to the energy of their binding to the tube. A nitrogen base is considered as stacked if more than half of pyrimidine or purine ring atoms are in van der Waals contact with the nanotube surface. Thus, to 10 ns, the energies of $r(C)_{25}$ and $r(I)_{25}$ binding to SWCNT reach 260 and 200 kcal/mol, respectively (Figure 8). This difference can be explained with a difference in the quantity of bases stacked to the tube surface: 13 cytosines of $r(C)_{25}$ and 9 hypoxanthines of $r(I)_{25}$. In addition, to 10 ns, $r(I)_{25}$ formed two loops being characterized with the appearance of H-bonds between two hypoxanthines, which are located on the opposite sides of this loop (Figure 9).

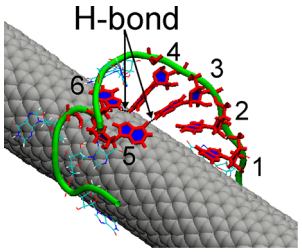

Figure 9. Snapshots of the loop formed by $r(I)_{25}$ on the tube surface after a 60 ns simulation. The phosphate backbone is depicted by a green solid curve, ribose and base rings are shown by blue color, and some nucleotides (bold red structures) form H-bonding dimers (3−5, 4−6) created inside the loop.

Note that such a strong loop strengthening is possible just as a result of the oligomer base disordering. On the contrary, the loops being formed by $r(C)_{25}$ up to 10 ns did not demonstrate the appearance of H-bonds inside the loop because of the base ordering which hinders the essential oligomer distortion to promote such bond appearance.

Next, the 10 ns simulation showed a noticeable growth of the interaction energy of $r(C)_{25}$, while for $r(I)_{25}$ the energy increase

dx.doi.org/10.1021/jp311005y | J. Phys. Chem. B 2013, 117, 2636−2644

was essentially weaker. After 20 ns simulation, the binding energy reaches 290 and 230 kcal/mol for $r(C)_{25}$ and $r(I)_{25}$, respectively (Table 1). The difference in the energy values

Table 1. Number of Nitrogen Bases of Oligonucleotides $r(C)_{25}$ and $r(I)_{25}$, Stacked with the Tube Surface, and the Energy Value of Oligomer Binding to the Tube Surface for Various Simulation Times

time	type of nitrogen base stacking	$r(I)_{25}$	$r(C)_{25}$
20 ns	stacked with tube	10 hypoxanthines (220 kcal/mol)	15 cytosines (290 kcal/mol)
	unstacked	loop	loop
40 ns	stacked with tube	13 hypoxanthines (240 kcal/mol)	19 cytosines (305 kcal/mol)
	unstacked	loop	2 dimers
60 ns	stacked with tube	13 hypoxanthines (250 kcal/mol)	19 cytosines (325 kcal/mol)
	unstacked	loop (7 hypoxanthines)	loop

correlates with the number of bases stacked to the nanotube surface: 15 cytosines and 10 hypoxanthines. In the next 10 ns simulation, the binding energies do not change essentially.

After 40 ns simulation, the number of cytosines stacked with the nanotube reaches 19, but $r(I)_{25}$ demonstrates only 13 hypoxanthines in stacking with the nanotube. It follows from Table 1 that this number of stacked bases keeps until the simulation finishes. The dependence of the energy of $r(I)_{25}$ binding to the tube on time shows a tendency with small increasing energy, while this energy for SWCNT:$r(C)_{25}$ increases more essentially. Finally, until 60 ns simulation, the binding energy reaches 325 and 250 kcal/mol for $r(C)_{25}$ and $r(I)_{25}$, respectively. The loop formed by $r(I)_{25}$ on the nanotube remains until 60 ns of simulation (Figure 6), while the $r(C)_{25}$ loop disappears with time.

Upon $r(C)_{25}$ adsorption on the nanotube surface, domains of self-stacked bases are kept rather long. Most likely, just these domains promote keeping of the helix structure of the whole oligomer. In comparison with $r(C)_{25}$, disordered $r(I)_{25}$ is lesser elongated along the nanotube, and the loop formed makes its position on the tube more compact.

The principal difference between simulation of our polymer adsorption on the nanotube and earlier modeled polymer (stiff or flexible) lays in their different structures. Thus, in previous studies, rigidity or flexibility of the polymer was mainly provided by the polymer backbone. In our case, the backbone of two biopolymers was the same (the sugar−phosphate one), and the polymer inflexibility depends on the value of the base self-stacking interaction. As adsorption of the polymer takes place mainly through bases, just the absorption reduces this difference in flexibility. This essential difference permits one to distinguish adsorption of organic polymers onto the nanotube from DNA/RNA adsorption.

CONCLUSIONS

We have compared the adsorption properties of homopolynucleotides poly(rI) and poly(rC) on the SWCNT surface, employing UV spectroscopy with analysis of absorption spectra at room temperature as well as at heating (until 90 °C) of the hybrid aqueous suspension obtained and MD simulations that explore mechanisms of spontaneous helix oligomer adsorption on the nanotube surface, hybrid structure, and energetic properties of SWCNT:$r(C)_{25}$ and SWCNT:$r(I)_{25}$. We showed that adsorption of the poor base stacked helix poly(rI) onto the nanotube in aqueous suspension is less effective than that of the strong base stacked poly(rC), the chain of which is of higher rigidity. Heating of the nanotube:polymer aqueous suspension until 90 °C, which leads to partial nanotube aggregation and precipitation because of weakly bound polymer sliding from the tube surface, revealed that a part of the precipitated nanotubes, determined from the analysis of absorption spectra of the nanotube suspensions, is about 2.3 larger for the SWCNT:poly(rI) suspension than for SWCNT:poly(rC). Adsorption of polymer (poly(rI)) on the nanotube surface is accompanied with a red-shift (∼5 nm) of the band maximum in the polymer absorption spectrum similarly as it was observed earlier[30] under adsorption of some homodeoxyoligonucleotides on SWCNT.

MD modeling demonstrated that oligomer $r(I)_{25}$ has an essentially weaker energy of binding to the carbon nanotube surface than $r(C)_{25}$ (250 kcal/mol vs 325 kcal/mol). Such a huge difference in the energies of the oligomer binding to the tube surface is explained by a smaller number of NBs (hypoxanthines) of the first oligonucleotide π-stacked with the tube surface than of the second one (13 vs 19) in spite of purines exhibiting the stronger binding than pyrimidines (cytosine).[27] Structural analysis of oligomers on the nanotube surface revealed that the more ordered oligomer is of tendency to the stretched conformation along the nanotube. On the contrary, a higher flexibility of $r(I)_{25}$ leads to the formation of a stable loop kept away from the nanotube surface. The stability of this loop is strengthened with H-bonding between bases located in different loop sides. Thus, the different base ordering/flexibility of ss-RNA (or ss-DNA) enables one to obtain a wide range of polymer wrapping conformations around the SWCNT. The obtained results offer the challenge for practical use of homooligonucleotides to solubilize and separate carbon nanotubes, for photophysics of semiconducting SWCNTs as the polymer ordering on the nanotube effects on the electronic structure of nanotubes, and for creating carbon nanotube self-assembled multicomponent structures for SWCNT-based electronic devices.

AUTHOR INFORMATION

Corresponding Author

*Phone: +380 57 340 1595. Fax: +380 57 340 2370. E-mail: mkarachevtsev@ilt.kharkov.ua.

Notes

The authors declare no competing financial interest.

ACKNOWLEDGMENTS

We are grateful to Dr. L. F. Belous for useful consultation at all simulation stages. Also, the authors acknowledge the Computational Center at B. I. Verkin Institute for Low Temperature Physics and Engineering for providing computer time.

REFERENCES

(1) O'Connell, M. J.; Boul, P.; Ericson, L. M.; Huffman, Ch.; Wang, Y.; Haros, E.; Kuper, C.; Tour, J.; Ausman, K. D.; Smalley, R. E. Reversible Water-Solubilization of Single-Walled Carbon Nanotubes by Polymer Wrapping. *Chem. Phys. Lett.* **2001**, *342*, 265−271.

(2) Imin, P.; Cheng, F.; Adronov, A. Supramolecular Complexes of Single Walled Carbon Nanotubes with Conjugated. Polymers. *Polym. Chem.* **2011**, *2*, 411−416.

(3) Zheng, M.; Jagota, A.; Semke, E. D.; Diner, B. A.; McLean, R. S.; Lustig, S. R.; Richardson, R. E.; Tassi, N. G. DNA-Assisted Dispersion and Separation of Carbon Nanotubes. *Nat. Mater.* **2003**, *2*, 338−342.
(4) Haggenmueller, R.; Rahatekar, S. S.; Fagan, J. A.; Chun, J. H.; Becker, M. L.; Naik, R. R.; Krauss, T.; Carlson, L.; Kadla, J. F.; Trulove, P. C.; Fox, D. F.; DeLong, H. C.; Fang, Z.; Kelley, S. O.; Gilman, J. W. Comparison of the Quality of Aqueous Dispersions of Single Wall Carbon Nanotubes Using Surfactants and Biomolecules. *Langmuir* **2008**, *24*, 5070−5078.
(5) Star, A.; Stoddart, J. F.; Steuerman, D.; Diehl, M.; Boukai, A.; Wong, E. W.; Yang, X.; Chung, S.-W.; Choi, H.; Health, J. R. Preparation and Properties of Polymer-Wrapped Single-Walled Carbon Nanotubes. *Angew. Chem., Int. Ed.* **2001**, *40*, 1721−1725.
(6) Yang, M.; Koutsos, V.; Zaiser, M. Interactions between Polymers and Carbon Nanotubes: A Molecular Dynamics Study. *J. Phys. Chem. B* **2005**, *109*, 10009−10014.
(7) Kusner, I.; Srebnik, S. Conformational Behavior of Semi-flexible Polymers Confined to a Cylindrical Surface. *Chem. Phys. Lett.* **2006**, *430*, 84−88.
(8) Gurevitch, I.; Srebnik, S. Conformational Behavior of Polymers Adsorbed on Nanotubes. *J. Chem. Phys.* **2008**, *128*, 144901-1−144901-8.
(9) Tallury, S. S.; Pasquinelli, M. A. Molecular Dynamics Simulations of Flexible Polymer Chains Wrapping Single-Walled Carbon Nanotubes. *J. Phys. Chem. B* **2010**, *114*, 4122−4129.
(10) Tallury, S. S.; Pasquinelli, M. A. Molecular Dynamics Simulations of Polymers with Stiff Backbones Interacting with Single-Walled Carbon Nanotubes. *J. Phys. Chem. B* **2010**, *114*, 9349−9355.
(11) Rotkin, S. V. Electronic Properties of Nonideal Nanotube Materials: Helical Symmetry Breaking in DNA Hybrids. *Annu. Rev. Phys. Chem.* **2010**, *61*, 241−261.
(12) Meng, S.; Maragakis, P.; Papaloukas, C.; Kaxiras, E. DNA Nucleoside Interaction and Identification with Carbon Nanotubes. *Nano Lett.* **2007**, *7*, 45−50.
(13) Zhang, J.; Boghossian, A. A.; Barone, P. W.; Rwei, A.; Kim, J.-H.; Lin, D.; Heller, D. A.; Hilmer, A. J.; Nair, N.; Reuel, N. F.; et al. Single Molecule Detection of Nitric Oxide Enabled by $d(AT)_{15}$ DNA Adsorbed to Near Infrared Fluorescent Single-Walled Carbon Nanotubes. *J. Am. Chem. Soc.* **2011**, *133* (3), 567−581.
(14) Frischknecht, A. L.; Martin, M. G. Simulation of the Adsorption of Nucleotide Monophosphates on Carbon Nanotubes in Aqueous Solution. *J. Phys. Chem. C* **2008**, *112*, 6271−6278.
(15) Karachevtsev, V. A.; Gladchenko, G. O.; Karachevtsev, M. V.; Valeev, V. A.; Leontiev, V. S.; Lytvyn, O. S. Adsorption of Poly(rA) on the Carbon Nanotube Surface and Its Hybridization with Poly(rU). *Chem. Phys. Phys. Chem.* **2008**, *9*, 2010−2018.
(16) Martin, W.; Zhu, W.; Krilov, G. Simulation Study of Noncovalent Hybridization of Carbon Nanotubes by Single-Stranded DNA in Water. *J. Phys. Chem. B* **2008**, *112*, 16076−16089.
(17) Karachevtsev, M. V.; Lytvyn, O. S.; Stepanian, S. G.; Leontiev, V. S.; Adamowicz, L.; Karachevtsev, V. A. SWNT-DNA and SWNT-polyC Hybrids: AFM Study and Computer Modeling. *J. Nanosci. Nanotechnol.* **2008**, *8*, 1473−1480.
(18) Johnson, R. R.; Johnson, A. T. C.; Klein, M. L. Probing the Structure of DNA−Carbon Nanotube Hybrids with Molecular Dynamics. *Nano Lett.* **2008**, *8*, 69−75.
(19) Johnson, R. R.; Kohlmeyer, A.; Johnson, A. T. C.; Klein, M. L. Free Energy Landscape of a DNA−Carbon Nanotube Hybrid Using Replica Exchange Molecular Dynamics. *Nano Lett.* **2009**, *9*, 537−541.
(20) Johnson, R. R.; Johnson, A. T. C.; Klein, M. L. The Nature of DNA-Base−Carbon-Nanotube Interactions. *Small* **2010**, *6*, 31−34.
(21) Roxbury, D.; Manohar, S.; Jagota, A. Molecular Simulation of DNA β-Sheet and β-Barrel Structures on Graphite and Carbon Nanotubes. *J. Phys. Chem. C* **2010**, *114*, 13267−13276.
(22) Roxbury, D.; Mittal, J.; Jagota, A. Molecular-Basis of Single-Walled Carbon Nanotube Recognition by Single-Stranded DNA. *Nano Lett.* **2012**, *12*, 1464−1469.
(23) Karachevtsev, M. V.; Karachevtsev, V. A. Peculiarities of Homooligonucleotides Wrapping around Carbon Nanotubes: Molecular Dynamics Modeling. *J. Phys. Chem. B* **2011**, *115*, 9271−9279.
(24) Bobadilla, A. D.; Seminario, J. M. DNA−CNT Interactions and Gating Mechanism Using MD and DFT. *J. Phys. Chem. C* **2011**, *115*, 3466−3474.
(25) Tu, X.; Manohar, S.; Jagota, A.; Zheng, M. DNA Sequence Motifs for Structure-Specific Recognition and Separation of Carbon Nanotubes. *Nature* **2009**, *460*, 250−253.
(26) Gowtham, S.; Scheicher, R. H.; Pandey, R.; Karna, S. P.; Ahuja, R. First-principles Study of Physisorption of Nucleic Acid Bases on Small-Diameter Carbon Nanotubes. *Nanotechnology* **2008**, *19*, 125701−125718.
(27) Stepanian, S. G.; Karachevtsev, M. V.; Glamazda, A. Yu.; Karachevtsev, V. A.; Adamowicz, L. Raman Spectroscopy Study and First-Principles Calculations of the Interaction between Nucleic Acid Bases and Carbon Nanotubes. *J. Phys. Chem. A* **2009**, *113*, 3621−3629.
(28) Shukla, M. K.; Dubey, M.; Zakar, E.; Namburu, R.; Czyznikowska, Z.; Leszczynski, J. Interaction of Nucleic Acid Bases with Single-Walled Carbon Nanotube. *Chem. Phys. Lett.* **2009**, *480*, 269−272.
(29) Hughes, J. M; Cathcart, H.; Coleman, J. N. Dispersion and Exfoliation of Nanotubes with Synthetic Oligonucleotides: Variation of Dispersion Efficiency and Oligo-Nanotube Interaction with Base Type. *J. Phys. Chem. C* **2010**, *114*, 11741−11747.
(30) Hughes, M. E.; Brandin, E.; Golovchenko, J. A. Optical Absorption of DNA−Carbon Nanotube Structures. *Nano Lett.* **2007**, *7*, 1191−1194.
(31) Tinoco, I., Jr. Hypochromism in Polynucleotides. *J. Am. Chem. Soc.* **1960**, *82*, 4785−4790.
(32) Cantor, C. R.; Schimmel, P. R. *Biophysical Chemistry*; W.N. Freeman and Company: San Francisco, CA, 1980.
(33) Karachevtsev, V. A.; Plokhotnichenko, A. M.; Karachevtsev, M. V.; Leontiev, V. S. Decrease of Carbon Nanotube UV Light Absorption Induced by $\pi-\pi$-Stacking Interaction with Nucleotide Bases. *Carbon* **2010**, *48*, 3682−3691.
(34) Freier, S. M.; Hill, K. O.; Dewey, T. G.; Marky, L. A.; Breslauer, K. J.; Turner, D. H. Solvent Effects on the Kinetics and Thermodynamics of Stacking in Poly(Cytidylic Acid). *Biochemistry* **1981**, *20*, 1419−1426.
(35) Fasman, G. D.; Lindblow, C.; Grossman, L. The Helical Conformations of Polycytidylic Acid: Studies on the Forces Involved. *Biochemistry* **1964**, *3* (8), 1015−1021.
(36) Brahms, J.; Maurizot, J. C.; Michelson, A. M. Conformation and Thermodynamic Properties of Oligocytidilic Acids. *J. Mol. Biol.* **1967**, *25*, 465−480.
(37) Thiele, D.; Guschlbauer, W. The Structures of Polyinosinic Acid. *Biophysik* **1973**, *9*, 261−277.
(38) Cech, C. L.; Tinoco, I., Jr. Circular Dichroism Calculations for Polyinosinic Acid in Proposed Multi-Stranded Geometries. *Nucleic Acids Res.* **1976**, *3*, 399−404.
(39) Howard, F. B.; Miles, H. T. Poly(inosinic acid) Helixes: Essential Chelation of Alkali Metal Ions in the Axial Channel. *Biochemistry* **1982**, *21*, 6736−6745.
(40) Albertorio, F.; Hughes, M. E.; Golovchenko, J. A.; Branton, D. Base Dependent DNA−Carbon Nanotube Interactions: Activation Enthalpies and Assembly−Disassembly Control. *Nanotechnology* **2009**, *20*, 395101.
(41) Phillips, J. C.; Braun, R.; Wang, W.; Gumbart, J.; Tajkhorshid, E.; Villa, E.; Chipot, Ch.; Skeel, R. D.; Kale, L.; Schulten, K. Scalable Molecular Dynamics with NAMD. *J. Comput. Chem.* **2005**, *26*, 1781−1802.
(42) Foloppe, N.; MacKerell, A. D., Jr. All-Atom Empirical Force Field for Nucleic acids: I. Parameter Optimization Based on Small Molecule and Condensed Phase Macromolecular Target Data. *J. Comput. Chem.* **2000**, *21*, 86−104.
(43) http://structure.usc.edu/make-na/server.html.
(44) Humphrey, W.; Dalke, A.; Schulten, K. VMD: Visual Molecular Dynamics. *J. Mol. Graphics* **1996**, *14*, 33−38.

(45) Bloomfield, V. A.; Crothers, D. M.; Tinoco, I., Jr. *Nucleic Acids. Structures, Properties and Functions*; University Science Books: Sausalito, CA, 2000.
(46) Seol, Y.; Skinner, G. M.; Visscher, K.; Buhot, A.; Halperin, A. Stretching of Homopolymeric RNA Reveals Single-Stranded Helices and Base-Stacking. *Phys. Rev. Lett.* **2007**, *98*, 158103-1−158103-4.